Johann Radon Institute for
Computational and Applied Mathematics
Austrian Academy of Sciences (ÖAW)

A parallel multigrid solver for multi-patch Isogeometric Analysis

C. Hofer, S. Takacs

RICAM-Report 2018-10

A parallel multigrid solver for multi-patch Isogeometric Analysis

Christoph Hofer and Stefan Takacs

Abstract Isogeometric Analysis (IgA) is a framework for setting up spline-based discretizations of partial differential equations, which has been introduced around a decade ago and has gained much attention since then. If large spline degrees are considered, one obtains the approximation power of a high-order method, but the number of degrees of freedom behaves like for a low-order method. One important ingredient to use a discretization with large spline degree, is a robust and preferably parallelizable solver. While numerical evidence shows that multigrid solvers with standard smoothers (like Gauss Seidel) does not perform well if the spline degree is increased, the multigrid solvers proposed by the authors and their co-workers proved to behave optimal both in the grid size and the spline degree. In the present paper, the authors want to show that those solvers are parallelizable and that they scale well in a parallel environment.

1 Introduction

Isogeometric Analysis (IgA) was originally introduced in the seminal paper [10], aiming to unite the worlds of computer aided design (CAD) and finite element (FEM) simulation. From a technical point of view, it is a framework for setting up spline-based discretizations of partial differential equations. The key idea is that the spline space is typically first defined on the unit square or the unit cube and then mapped to the computational domain using one global geometry function. More complicated domains cannot be represented by just one such geometry function. In-

Christoph Hofer
Doctoral Program Computational Mathematics, University Linz, Altenberger Str. 69, 4040 Linz, e-mail: christoph.hofer@dkcm.jku.at

Stefan Takacs
RICAM, Austrian Academy of Sciences, Altenberger Str. 69, 4040 Linz, e-mail: stefan.takacs@ricam.oeaw.ac.at

stead, the computational domain is decomposed into patches, where each of them is represented by its own geometry function. This is called the *multi-patch case*, in contrast to the *single-patch case*.

As a next step, the linear system resulting from the discretization of the PDE has to be solved. This might be challenging as the condition number of the linear system grows exponentially with the spline degree, where high spline degrees might be desired because of their superior approximation power.

While in early IgA literature, the dependence of methods on the spline degree has not been considered, in the last few years robustness in the spline degree has gained increasing interest. Several (almost) robust approaches or approaches with a mild dependence on the spline degree have been proposed, on the one side for the single-patch case, cf. [2, 5, 9, 12, 8] and references therein, and on the other side as approaches aiming to combine patch-local solvers to a global solver, cf. [11, 3, 4, 1] and references therein.

In [13], we have considered a slightly different approach: We do not aim to combine patch-local solvers to a global solver, but to combine patch-local smoothers to a global smoother which is used within a global multigrid solver. In the present paper, we give some additional remarks on an efficient implementation of the multigrid method, comment on its parallelization and give numerical results.

This paper is organized as follows. First, the model problem and the discretization are discussed in Sec. 2. Then, in Sec. 3, we recall the formulation of the multigrid solver. Its parallelization is discussed in the following Sec. 4. In Sec. 5, we give the results of numerical experiments and draw conclusions.

2 Model problem and isogeometric discretization

Let $\Omega \subset \mathbb{R}^d$ with $d \in \{2,3\}$ be a bounded computational domain with Lipschitz boundary. We consider a standard *Poisson model problem*

$$-\Delta u = f \quad \text{in} \quad \Omega\,, \quad u = 0 \quad \text{on} \quad \Gamma_D \qquad \text{and} \qquad \frac{\partial u}{\partial n} = 0 \quad \text{on} \quad \Gamma_N\,,$$

where Γ_D is a subset of $\partial\Omega$ with positive measure and $\Gamma_N := \partial\Omega \backslash \Gamma_D$. The model problem reads in variational form as follows. Given $f \in L_2(\Omega)$, find $u \in H^1_{0,D}(\Omega)$ such that

$$(\nabla u, \nabla v)_{L_2(\Omega)} = (f, v)_{L_2(\Omega)} \qquad \text{for all} \quad v \in H^1_{0,D}(\Omega)\,. \tag{1}$$

Here and in what follows, $L_2(\Omega)$ and $H^1(\Omega)$ are the standard Lebesgue and Sobolev spaces with standard norms and $H^1_{0,D}(\Omega) := \{u \in H^1(\Omega) \,:\, u|_{\Gamma_D} = 0\}$.

We preform a standard isogeometric multi-patch discretization as it has been specified in [13]. In the present paper, we try to keep the explanation short and give only an overview. We assume that the computational domain Ω is composed of K patches Ω_k such that

$$\overline{\Omega} = \bigcup_{k=1}^{K} \overline{\Omega_k} \quad \text{and} \quad \Omega_k \cap \Omega_l = \emptyset \text{ for any } k \neq l \ , \tag{2}$$

where each patch Ω_k is a bounded and open domain. We assume that the patches are fully matching, i.e., the intersections $\overline{\Omega_k} \cap \overline{\Omega_l}$ are either empty, common vertices, common edges or common faces. Any of the patches is parametrized by a bijective geometry function

$$\mathbf{G}_k : \widehat{\Omega} := (0,1)^d \to \Omega_k := \mathbf{G}_k(\widehat{\Omega}) \subset \mathbb{R}^d \ .$$

Before we define set of trial functions $V_\ell \subset H^1_{0,D}(\Omega)$, we introduce discretizations living on the parameter domain $\widehat{\Omega}$. Let

$$S_{p,h}(0,1) := \left\{ u \in C^{p-1}(0,1) \ : \ u|_{[hi,h(i+1)]} \text{ is a polynomial of degree } p \ , \ \forall_{i=1,\dots,n} \right\}$$

be the space of univariate splines of maximum smoothness and the space $S_{p,h}(\widehat{\Omega}) := S_{p,h}(0,1) \otimes \cdots \otimes S_{p,h}(0,1)$ be the corresponding tensor-product spline space. The grid size h and the spline degree p might be different for any patch and for any spacial direction; for simplicity, we do not express that in the notation. Based on the discretization living on the parameter domain $\widehat{\Omega}$, we define the function space V_ℓ of isogeometric functions living on the physical domain Ω as follows:

$$V_\ell := \{ u \in C^0(\Omega) \ : \ u \circ \mathbf{G}_k \in S_{p,h_\ell}(\widehat{\Omega}) \} \ . \tag{3}$$

We assume to have a *fully matching discretization*, which means that the discretizations agree on the interfaces. A more formal definition of the basis and its discretization is given in [13, Sec. 2]. In Fig. 1, a fully matching discretization is depicted, where each node represents one basis function and therefore one degree of freedom (dof). Note that any of the basis function whose associated node lies on one patch, vanishes outside of that patch. Any of the basis functions whose associated node lies within one edge, vanishes outside the union of the edge and the adjacent patches. Finally, any of the basis functions whose associated node coincides with one vertex, vanishes outside the union of that vertex and the adjacent edges and patches. The behavior in three dimensions is completely analogous.

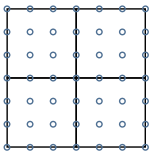

Fig. 1: Fully matching discretization

The Galerkin principle yields the following discretized variational problem. Find $u \in V_\ell$ such that

$$a(u,v) = (f,v)_{L_2(\Omega)} \qquad \text{for all } v \in V_\ell \,, \tag{4}$$

where

$$a(u,v) := (\nabla u, \nabla v)_{L_2(\Omega)} = \sum_{k=1}^{K} \underbrace{(|\det J_{\mathbf{G}_k}| J_{\mathbf{G}_k}^{-\top} J_{\mathbf{G}_k}^{-1} \nabla \widehat{u}_k, \nabla \widehat{v}_k)_{L^2(\widehat{\Omega})}}_{a_k(u,v) :=} \tag{5}$$

for $\widehat{u}_k := u \circ \mathbf{G}_k \in S_{p,h_\ell}(\widehat{\Omega})$ and $\widehat{v}_k := v \circ \mathbf{G}_k \in S_{p,h_\ell}(\widehat{\Omega})$ and where $J_{\mathbf{G}_k}$ is the Jacobian of the geometry map. Using the chosen basis, we obtain a matrix-vector formulation of the discretized problem, which reads as follows. Find $\underline{u} \in \mathbb{R}^N$ such that

$$A_\ell \, \underline{u} = \underline{f} \,. \tag{6}$$

Allowing constants that depend on the geometry function, we obtain that the matrix A_ℓ is spectrally equivalent to the matrix $\widehat{A}_\ell$, which discretizes the bilinear form

$$\widehat{a}(u,v) := \sum_{k=1}^{K} (\nabla \widehat{u}_k, \nabla \widehat{v}_k)_{L^2(\widehat{\Omega})} \,,$$

where, again, $\widehat{u}_k := u \circ \mathbf{G}_k$ and $\widehat{v}_k := v \circ \mathbf{G}_k$.

3 The multigrid solver and its extension to three dimensions

We employ the multigrid solver based on a hierarchy of grids for grid levels $\ell = 0, \dots, L$, obtained by uniform refinement. Throughout the grid hierarchy, the spline degree p and the corresponding smoothness is kept unchanged. This yields nested spaces: $V_0 \subset V_1 \subset \cdots \subset V_L \subset H^1_{0,D}(\Omega)$, which allows to use the canonical embedding $V_{\ell-1} \to V_\ell$ for the multigrid method; its matrix representation is denoted by P_ℓ. Following the usual pattern, we use its transpose $P_\ell^\top$ as restriction.

One *multigrid cycle* on some grid level ℓ consists of the following steps.

- First, ν *pre-smoothing steps* are applied, where each reads as follows:

$$\underline{u} \leftarrow \underline{u} + \tau L_\ell^{-1} (\underline{f} - A_\ell \underline{u}) \,. \tag{7}$$

  The choice of the smoothing operator L_ℓ^{-1} and the damping parameter τ are discussed below.
- Then, the *coarse grid correction* is performed:

$$\underline{u} \leftarrow \underline{u} + \tau P_\ell A_{\ell-1}^{-1} P_\ell^\top (\underline{f} - A_\ell \underline{u}) \,,$$

where for $\ell > 1$, the application $A_{\ell-1}^{-1}$ is replaced by $\mu = 1$ (V-cycle) or $\mu = 2$ (W-cycle) recursive applications of the multigrid method on the coarser grid level.
- Finally, again ν *post-smoothing steps* (7) are applied.

As smoother, an additive Schwarz type combination

$$L_\ell^{-1} := \sum_T P_{\ell,T} L_{\ell,T}^{-1} P_{\ell,T}^\top \tag{8}$$

of local smoothing operators $L_{\ell,T}^{-1}$ is proposed, where the dofs are collected based on separating the domain into *pieces*: patches, vertices, edges and, in three dimensions, faces. Here, each dof is assigned to exactly one of these pieces, cf. Fig. 2. Certainly, based on such a one-by-one splitting, the matrix $P_{\ell,T}$ is nothing but a indicator matrix representing the canonical embedding.

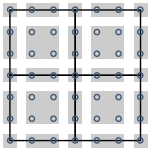

Fig. 2: Decomposition into pieces serving as subspaces for the additive Schwarz method

The local smoothing operators are chosen as follows.

- For the patch-interiors, the subspace corrected mass smoother as proposed in [8] is chosen as smoothing operator $L_{\ell,T}^{-1}$.
- For the edges and vertices, in [13] direct solvers have been proposed as smoothers, i.e., $L_{\ell,T}$ is the restriction of the matrix A_ℓ to the edge or vertex. To avoid unnecessary communication, we choose an approximation which can be computed directly. Using [13, Lemma 4.1] and [13, eq. (4.16)], we obtain that the restriction of A_ℓ to an edge is spectrally equivalent to

$$L_{\ell,T} := \left(\frac{h_\ell}{p}\right)^{d-1} \mathrm{K}_\ell + \left(\frac{h_\ell}{p}\right)^{d-3} \mathrm{M}_\ell \,,$$

where K_ℓ and M_ℓ are the corresponding univariate stiffness and mass matrices. Analogously, its restriction to a vertex is a constant in the order of

$$L_{\ell,T} := \left(\frac{h_\ell}{p}\right)^{d-2} .$$

- Three dimensional problems have not been considered in [13], so we have to discuss how to choose the local smoothers for faces. If, as for the edges and vertices, again a direct solver was applied, the overall computational costs would

not be optimal anymore. So, again, observe that the the restriction of A_ℓ to a face is spectrally equivalent to

$$L^*_{\ell,T} := \left(\frac{h_\ell}{p}\right)^{d-2} \mathscr{K}_\ell + \left(\frac{h_\ell}{p}\right)^{d-4} \mathscr{M}_\ell \,,$$

where and $\mathscr{K}_\ell = \mathrm{K}_\ell \otimes \mathrm{M}_\ell + \mathrm{M}_\ell \otimes \mathrm{K}_\ell$ and $\mathscr{M}_\ell = \mathrm{M}_\ell \otimes \mathrm{M}_\ell$ are the corresponding stiffness and mass matrices on the face. For $d = 3$, we obtain

$$L^*_{\ell,T} = \frac{h_\ell}{p}\left(\mathscr{K}_\ell + \frac{p^2}{h_\ell^2}\mathscr{M}_\ell\right) .$$

Here, analogously to the case of the patch-interiors, the subspace corrected mass smoother is used. Note that the subspace corrected mass smoother is set up such that it bounds the stiffness matrix $\mathscr{K}_\ell$ from above, cf. [8, eq. (11)]. In the present paper, besides a trivial scaling, the stiffness matrix $\mathscr{K}_\ell$ is augmented by $p^2 h_\ell^{-2}$ times the mass matrix $\mathscr{M}_\ell$. So, we have also to augment the local contributions for the subspace corrected mass smoother, cf. the matrices L_α in [8, Sec. 4.2], in the same way.

4 The parallelization of the multigrid solver

The parallelization of the multigrid solver follows the approach presented in [6]. We use MPI[1], so each processor executes independently the whole algorithm with its local data until communication is explicitly requested.

We assign each of the patches to one of the processors. So, that processor holds the values of all dofs that belong to that patch including its interfaces, cf. Fig. 3. This means that the dofs on the interfaces might be assigned to more than one processor.

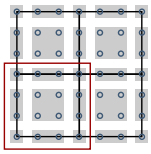

Fig. 3: The distribution of the dofs to the processors

A vector that occurs in the algorithm, say $\underline{w}$, is stored either in accumulated form (Type I) or distributed form (Type II). We say that a vector is stored in accumulated form if each of the processors holds those parts of the global vector which correspond to the dofs assigned to the processor. We denote such vectors by $\underline{w}_{acc}$.

[1] Message Passing Interface, see http://mpi-forum.org/.

We say that a vector is stored in distributed form if the global vector is the sum of the contributions of all the processors. Such vectors are denoted by $\underline{w}_{dist}$. Again, the processor-local contributions of the distributed vectors are supported only the patches assigned to the processor including their interfaces.

Note that only certain kinds of operations make sense; so we can add accumulated and distributed vectors only to vectors of the same type:

$$\underline{u}_{acc} + \underline{v}_{acc} \to \underline{w}_{acc} \quad \text{and} \quad \underline{u}_{dist} + \underline{v}_{dist} \to \underline{w}_{dist} \ ,$$

cf. [6, Sec. 5.3]. As the multi-patch setting is equivalent to a standard approach of non-overlapping domain decomposition, the overall stiffness matrix is assembled on a per-patch basis, i.e., the bilinear forms a_k from (5) are evaluated separately yielding matrices $A_{\ell,k}$. Consequently, the global stiffness matrix A_ℓ is the sum of the local contributions $A_{\ell,k}$. This means that the matrix A_ℓ is stored in distributed form, which yields the following mapping type:

$$A_\ell \, \underline{u}_{acc} \to \underline{w}_{dist} \ ,$$

i.e., A_ℓ can be applied to accumulated vectors and the the result of the operation is distributed, cf. [6, Sec. 5.4.1].

Similar to [6, Sec. 7.2.2], the inter-grid transfer operators satisfy

$$P_\ell \, \underline{u}_{acc} \to \underline{w}_{acc} \quad \text{and} \quad P_\ell^\top \, \underline{u}_{dist} \to \underline{w}_{dist}$$

because the prolongation operator has a block-triangular structure as in [6, eq. (5.9)] and the restriction operator has a block-triangular structure as in [6, eq. (5.10)]. The block-triangular structure is obtained because the following statements hold true:

- On each vertex, the prolonged value $\underline{w}_{acc}$ coincides with the coarse-grid value $\underline{u}_{acc}$ of the same vertex.
- On each edge, the prolonged values $\underline{w}_{acc}$ only depend on the coarse-grid values $\underline{u}_{acc}$ on the same edge and on the adjacent vertices.
- On each patch-interior, the prolonged values $\underline{w}_{acc}$ only depend on the coarse-grid values $\underline{u}_{acc}$ on the same patch-interior and on the adjacent edges and vertices.

For three dimensions, completely analogous statements hold true.

The global operator L_ℓ^{-1} is block-diagonal, where each block corresponds to one piece. Note that by construction each piece belongs as a whole to one processor or is shared as a whole by the same processors, so it satisfies both the conditions of [6, eq. (5.9)] and [6, eq. (5.10)]. This shows

$$L_\ell^{-1} \, \underline{u}_{acc} \to \underline{w}_{acc} \quad \text{and} \quad L_\ell^{-1} \, \underline{u}_{dist} \to \underline{w}_{dist} \ ,$$

i.e., this operator can be applied both to distributed and accumulated vectors and it preserves the type of the vector.

As in any iterative solver, we need to accumulate the vectors of interest in each iterate. This we denote using the symbol Σ, which maps as follows:

$$\Sigma\, \underline{u}_{dist} \to \underline{w}_{acc}. \tag{9}$$

We note that only a communication between the processors holding neighboring patches is required in order to perform (9).

Only the coarsest grid level $\ell = 0$ needs some special treatment. Since the focus of the present paper is set on parallelizing the multigrid solver without changing its mathematical meaning, we perform an exact global solve on the coarsest grid level. This seems to be acceptable as it is done only for the coarsest grid level. So, we are required to communicate the stiffness matrix between all processors such that every processor holds a global stiffness matrix. We set up a direct solver A_0^{-1} for this global stiffness matrix, so its application is perform in the following way

$$\chi_{glob}\, A_0^{-1} \Sigma_{glob}\ \underline{u}_{acc} \to \underline{w}_{acc}\ ,$$

where Σ_{glob} denotes the accumulation of vectors where each processor obtains the global vector and χ_{glob} is the restriction of the global vector to the patches assigned to the processor. The latter involves only discarding unnecessary data. We obtain

$$\Sigma_{glob}\, \underline{u}_{dist} \to \underline{w}_{glob} \quad \text{and} \quad \chi_{glob}\, \underline{u}_{glob} \to \underline{w}_{acc}\ .$$

Overall, the parallel multigrid solver looks as follows:

Algorithm 1 Parallel multigrid solver

procedure MULTIGRID($\ell, \underline{u}_{acc}, \underline{f}_{dist}$)
  for all $i = 1, \dots, \nu$ **do** ▷ Pre-smoothing
    $\underline{u}_{acc} \leftarrow \underline{u}_{acc} + \tau \Sigma L_\ell^{-1}(\underline{f}_{dist} - A_\ell \underline{u}_{acc})$
  end for
  $\underline{r}_{dist} \leftarrow P_\ell^\top (\underline{f}_{dist} - A_\ell \underline{u}_{acc})$
  if $\ell = 1$ **then** ▷ Coarse-grid correction
    $\underline{p}_{acc} \leftarrow \chi_{glob}\, A_0^{-1} \Sigma_{glob}\, \underline{r}_{dist}$ ▷ Exact solver for coarsest grid level
  else
    $\underline{p}_{acc} \leftarrow 0$
    for all $i = 1, \dots, \mu$ **do** ▷ $\mu = 1$ is V-cycle; $\mu = 2$ is W-cycle
      $\underline{p}_{acc} \leftarrow$ MULTIGRID$(\ell - 1, \underline{p}_{acc}, \underline{r}_{dist})$
    end for
  end if
  $\underline{u}_{acc} \leftarrow \underline{u}_{acc} + P_\ell \underline{p}_{acc}$
  for all $i = 1, \dots, \nu$ **do** ▷ Post-smoothing
    $\underline{u}_{acc} \leftarrow \underline{u}_{acc} + \tau \Sigma L_\ell^{-1}(\underline{f}_{dist} - A_\ell \underline{u}_{acc})$
  end for
  return $\underline{u}_{acc}$
end procedure

We use our multigrid algorithm as a preconditioner for a standard parallel preconditioned conjugate gradient (PCG) solver. Note that the multigrid preconditioner already takes a distributed residual and returns an accumulated update. So, the pre-

conditioned conjugate gradient solver only needs to accumulate data in order to compute the required scalar products accordingly, cf. [6, Sec. 6.3.1].

5 Numerical experiments

In this section, we present numerical experiments concerning the parallelization of the multigrid solver. The solver was implemented in C++ based on the G+Smo library [7] and, as already mentioned, the parallelization is performed using MPI. All numerical experiments have been done using the HPC Cluster RADON1[2].

We present timings for setup, assembling and solving. The setup costs include

1. the costs of the setup of the dof-mappers, which describe the relation between the local dof-indices and the global dof-indices,
2. the costs of the grid refinement and the setup of the inter-grid transfer matrices,
3. the costs of the setup of the piece-local smoothers and
4. the costs of the setup of the coarse-grid solver.

Here, our implementation of item 1 requires that each processor knows about the indexing of the global dofs. Also for item 4, the information on all dofs is required, however only on the coarsest grid level. The costs which are typically dominant, i.e., those for assembling and for solving, are presented separately. It is important to note that assembling does not require the any kind of communication between the processors. So its parallelization is trivial. The communication, which is required for the solving phase, is discussed in detail in Sec. 4.

(a) The Yeti footprint

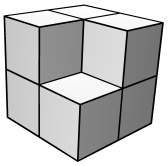

(b) The Fichera corner

Fig. 4: The computational domains

We have performed the numerical experiments for two and three dimensions. As two dimensional domain, we use the Yeti footprint (Fig. 4a), which has already been considered in [13] and which is also a popular domain for the IETI-DP method,

[2] We use up to 32 out of 68 available nodes, each equipped with 2x Xeon E5-2630v3 “Haswell” CPU (8 cores, 2.4 Ghz, 20 MB cache) and 128 GB RAM. More information is available at https://www.ricam.oeaw.ac.at/hpc/.

cf. [11]. As three dimensional domain, we consider the Fichera corner (Fig. 4b). This domain is often considered as extension of the L-shaped domain to three dimensions; the corresponding numerical experiments show that the proposed method can also be applied to domains without full elliptic regularity.

5.1 The Yeti footprint (2D)

On the Yeti footprint, we solve the model problem

$$\begin{aligned} -\Delta u &= 50\pi^2 \sin(5\pi\, x) \sin(5\pi\, y) && \text{in } \Omega\ , \\ u &= 0 && \text{on } \Gamma_D\ , \\ \frac{\partial}{\partial n} u &= 0 && \text{on } \Gamma_N\ , \end{aligned}$$

where Γ_D is the outer boundary and Γ_N are the four inner boundaries.

The Yeti footprint consists of 21 patches, which can be seen in Fig. 4a. Since we need sufficiently many patches for parallelization, we first split each patch uniformly into 16 patches, so we obtain in total $K = 336$ patches. We solve the problem with a conjugate gradient solver, preconditioned with one V-cycle of the multigrid method. We perform 1+1 smoothing steps of the proposed smoother. The damping parameter and the scaling parameter (in the subspace corrected mass smoother) are chosen as in [13], i.e., $\tau = 0.25$ and $\sigma = \frac{1}{0.2} h_\ell^{-2}$.

In Tab. 1, we report on the number of iterations required to reach the desired relative accuracy goal of 10^{-8}. Here, ℓ represents the number of refinement levels and p the spline degree. On the coarsest grid level ($\ell = 0$), the patch-local discretization only consists of global polynomials, i.e., each patch is one element of the discretization. Refinement is done by uniformly refining the patch-local grids, keeping the number of patches unchanged. We observe, as in [13], that the number of iterates is quite robust in the grid size and in the spline degree. The presented numbers have been computed with the serial code. The number of iterates is supposed to be the same if parallelization is applied; however due to some small numerical instabilities, in some cases the parallel code needs one additional iteration (but never more than that). Similar iteration counts are obtained for the W-cycle.

In Tab. 2, we present the strong scaling results. We fix the grid level ℓ and the spline degree p to two typical values. For $\ell = 7$ and $p = 4$, we have 5 768 189 dofs and the corresponding stiffness matrix has $4.6\ 10^8$ non-zero entries. For the case $\ell = 7$ and $p = 8$, the number of dofs increases slightly to 6 125 757, but the stiffness matrix has already $1.8\ 10^9$ non-zero entries. In the first two rows, we compare the costs of the serial code and the parallel code. Here, we obtain that the parallel code is slightly slower during the solving phase which is mainly due to the fact that the parallel code does not assemble the whole stiffness matrix but works with patch-local stiffness matrices. This allows also to consider the larger problem with $\ell = 7$ and $p = 8$, where the serial code caused memory problems.

$\ell \diagdown p$	2	3	4	5	6	7	8
4	45	42	37	33	31	28	25
5	48	44	40	36	33	30	27
6	50	44	41	36	35	33	27
7	51	45	42	37	36	34	28

Table 1: Iteration counts for Yeti footprint, $K = 336$

	$\ell = 7$, $p = 4$, $K = 336$						$\ell = 7$, $p = 8$, $K = 336$					
	Setup		Assembling		Solving		Setup		Assembling		Solving	
# Proc.	t	s	t	s	t	s	t	s	t	s	t	s
(serial)	217.1	–	522.1	–	4929.5	–	–	–	–	–	–	–
1	220.0	1	520.0	1	5125.9	1	549.0	1	8230.9	1	4729.8	1
2	80.1	2.7	263.8	1.9	1367.6	3.7	225.4	2.4	4158.5	1.9	1250.8	3.7
4	35.3	6.2	131.8	3.9	399.1	12.8	117.0	4.6	2098.5	3.9	409.9	11.5
8	17.1	12.8	66.0	7.8	109.6	46.7	53.9	10.1	1055.9	7.8	140.2	33.7
16	10.7	20.5	33.9	15.3	40.7	125.9	30.0	18.3	543.4	15.1	59.2	79.9
32	8.0	27.5	17.4	29.8	17.1	299.7	17.7	31.0	275.1	29.9	26.8	176.4
64	7.2	30.5	9.4	55.3	10.6	483.5	12.9	42.5	149.7	54.9	13.7	345.2
128	6.0	36.3	5.1	101.3	4.1	1250.2	9.9	55.4	76.2	108.0	7.2	656.9
256	6.3	34.4	3.2	160.0	3.3	1553.3	9.5	57.7	51.4	160.1	6.5	727.6

Table 2: Strong scaling behavior for Yeti footprint

	$\ell = 7$, $p = 4$					$\ell = 7$, $p = 8$				
# Proc.	# dofs	It.	Setup	Ass.	Solving	# dofs	It.	Setup	Ass.	Solving
4	360 902	46	1.4	9.2	7.9	383 262	46	6.6	147.3	21.4
16	1 442 569	44	2.4	9.3	8.5	1 531 977	44	8.7	151.2	20.8
64	5 768 189	41	7.2	9.5	10.5	6 125 757	28	13.2	148.7	13.7
256	23 068 573	36	42.4	9.7	9.5	24 498 717	26	54.5	153.8	20.0

Table 3: Weak scaling behavior for Yeti footprint

In the following rows, we consider the strong scaling behavior. We present in each case the time t in seconds required for setup, assembling and solving and the corresponding speedup s. We observe that the overall method has good strong scaling properties. As the setup phase consists also of parts that are not parallelized, we observe this time does not fall below a few seconds. The assembling phase, which is known to be dominant phase in high-order isogeometric methods, scales almost optimal. Also the solving phase needs rather little communication and is expected to scale well therefore. Indeed, the speedup is much larger than what would be expected. The authors think that this might be explained by some extraordinary caching effects, but here further investigation is required. The extraordinary well

behavior of the solver cannot be explained with changed convergence behavior because in all cases, the convergence behavior is identical.

In Tab. 3, we present weak scaling results. We again fix the grid level ℓ and the spline degree p to two typical values. Here, for the case of 4 processors, we consider the initial configuration of $K = 21$ patches; in the following rows we consider 84, 336 and 1344 patches. (So, the third row with 64 processors coincides with the line with 64 processors in Tab. 2.) As the setup phase is not fully parallelized, the setup times increase if the number of patches is increased. Both, the assembling times and the solving times are rather constant and do not indicate a clear tendency. The solving times also change due to the fact that the required number of iterations decays if the patches are split up. The computational costs for the global-coarse grid solver is negligible in this example; for $K = 1344$ patches the costs are 0.36 seconds for $p = 4$ and 1.4 seconds for $p = 7$ and for smaller patch numbers even less.

5.2 The Fichera corner (3D)

On the Fichera corner, we solve the model problem

$$\begin{aligned} -\Delta u &= 75\pi^2 \sin(5\pi\, x)\sin(5\pi\, y)\sin(5\pi\, z) && \text{in } \Omega := (0,2)^3\backslash[1,2)^3\ , \\ u &= 0 && \text{on } \Gamma_D := \{(x,y,z) \in \partial\Omega\ :\ xyz = 0\}\ , \\ \frac{\partial}{\partial n} u &= 0 && \text{on } \Gamma_N := \partial\Omega\backslash\Gamma_D\ . \end{aligned}$$

The Fichera corner consists of 7 patches, which can be seen in Fig. 4b, which are uniformly split into $K = 448$ patches in total. Again, we solve the problem with a conjugate gradient solver preconditioned with one V-cycle of the multigrid method with 1+1 smoothing steps. Again $\tau = 0.25$ and $\sigma = \frac{1}{0.2} h_\ell^{-2}$ are chosen.

In Tab. 4, we report on the number of iterations required to reach the desired relative accuracy goal of 10^{-8}. We observe, as for the Yeti footprint, that the number of iterates is quite robust in the grid size and in the spline degree. The presented numbers have been computed with the serial code. Again, the parallel code yields (almost) the same numbers.

In Tab. 5, we present the strong scaling results. For $\ell = 4$ and $p = 2$, we have $N = 2\,201\,024$ dofs and a stiffness matrix with $2.5\ 10^8$ non-zero entries. The second example with $\ell = 3$ and $p = 4$ yields $N = 596\,288$ dofs and $2.8\ 10^8$ non-zero entries. The timings behave similar as in the two-dimensional case, however the costs of the setup phase are much larger which can be explained by the fact that the interfaces are much larger. (For two dimensional problems, the interfaces consist of $\mathcal{O}(N^{1/2})$ dofs and for three dimensional problems, the interfaces consist of $\mathcal{O}(N^{2/3})$ dofs.) The assembling times seem to be optimal, whereas the solving times again behave extraordinary well.

In Tab. 6, we present weak scaling results. We again fix the grid level ℓ and the spline degree p to two typical values. Here, for the case of 4 processors, we consider

$\ell \diagdown p$	2	3	4	5	6
1	30	31	31	26	22
2	33	32	33	31	28
3	39	38	37	33	30
4	44	44	42	37	35

Table 4: Iteration counts for Fichera corner, $K = 448$

	$\ell = 4\ ,\ p = 2\ ,\ K = 448$						$\ell = 3\ ,\ p = 4\ ,\ K = 448$					
	Setup		Assembling		Solving		Setup		Assembling		Solving	
# Proc.	t	s	t	s	t	s	t	s	t	s	t	s
(serial)	179.4	–	260.2	–	4980.7	–	93.5	–	1313.5	–	1252.2	–
1	198.2	1	253.4	1	5091.3	1	109.7	1	1985.9	1	1073.1	1
2	77.7	2.5	127.4	1.9	1355.0	3.7	51.2	2.1	1103.3	1.8	340.0	3.1
4	49.2	4.0	63.5	3.9	395.7	12.8	30.6	3.5	492.2	4.0	110.2	9.7
8	32.9	6.0	32.0	7.9	99.2	51.3	22.8	4.8	214.1	9.2	40.1	26.7
16	28.3	7.0	16.5	15.3	34.4	148.0	27.3	4.0	113.4	17.5	22.7	47.2
32	26.8	7.4	8.4	30.1	12.4	410.5	17.0	6.4	55.5	35.7	8.3	129.2
64	32.2	6.1	5.5	46.0	5.0	1018.2	24.4	4.5	31.2	63.6	6.9	155.5
128	42.3	4.6	2.7	93.8	2.6	1958.1	15.8	6.9	15.4	128.9	3.6	298.0
256	54.1	3.6	1.1	230.3	1.8	2828.5	24.0	4.5	7.9	251.3	3.9	275.1

Table 5: Strong scaling behavior for Fichera corner

	$\ell = 4\ ,\ p = 2$					$\ell = 3\ ,\ p = 4$				
# Proc.	# dofs	It.	Setup	Ass.	Solving	# dofs	It.	Setup	Ass.	Solving
1	34 391	28	0.4	4.0	1.9	9 317	31	0.6	38.0	1.3
8	275 128	39	1.3	4.5	4.0	74 536	35	1.1	22.8	2.1
64	2 201 024	45	54.4	4.5	6.6	596 288	38	24.1	28.7	6.2
512	17 608 192	46	2071.3	5.1	11.1	4 770 304	35	2343.8	32.4	59.5

Table 6: Weak scaling behavior for Fichera corner

the initial configuration of $K = 7$ patches. For the following rows, we consider 56, 448 and 3584 patches. (So, the line with 64 processors coincides with the corresponding line in Tab. 5.) Again, the assembling times and the solving times do not show any clear tendency. Only for the last line with 3584 patches, the coarse-grid solver causes problems. For the case $\ell = 3$ and $p = 4$, 51 of the 59 seconds required for solving are due to the global solver on the coarsest grid. Again, the setup costs get dominant if the number of patches is increased.

Concluding, we have shown that the robust multi-patch multigrid solver from [13] can be extended to three dimensional domains and that it converges well also in this case. We have observed that the multigrid solver can be parallelized in a natural

way yielding very good speedup rates. Certainly, this is not the end of the story and further improvement should be considered in two directions. First, the setup phase becomes a bottleneck if many processors are considered. Here, improvements would be mainly a challenge in terms of implementation and data management. Second, the coarse-grid problem becomes too large if the number of patches is increased, particularly in the three dimensional case. To resolve that issue, it would be necessary to further coarsen the coarse-grid problem or to consider approximate solvers on the coarsest grid level which certainly would change the mathematical meaning of the algorithm and could, therefore, influence its convergence behavior. Finally, further investigation is required to completely understand the super optimal speedup rates observed in the strong scaling tests.

Acknowledgments. The first author would like to thank the Austrian Science Fund (FWF) for the financial support through the DK W1214-04, while the second author was supported by the FWF grant NFN S117-03.

References

1. S. Takacs C. Hofer, U. Langer, *Inexact dual-primal isogeometric tearing and interconnecting methods*, (2017), To appear in *Domain Decomposition Methods in Science and Engineering XXIV*. https://arxiv.org/abs/1705.04531.
2. N. Collier, D. Pardo, L. Dalcin, M. Paszynski, and V. M. Calo, *The cost of continuity: A study of the performance of isogeometric finite elements using direct solvers*, Comp. Meth. in Appl. Mech. Eng. **213–216** (2012), 353–361.
3. L. Beirão da Veiga, D. Cho, L. Pavarino, and S. Scacchi, *Overlapping Schwarz methods for isogeometric analysis*, SIAM Journal on Numerical Analysis **50** (2012), no. 3, 1394–1416.
4. L. Beirão da Veiga, L. F. Pavarino, S. Scacchi, O. B. Widlund, and S. Zampini, *Isogeometric BDDC preconditioners with deluxe scaling*, SIAM Journal on Scientific Computing **36** (2014), no. 3, A1118–A1139.
5. M. Donatelli, C. Garoni, C. Manni, S. Serra-Capizzano, and H. Speleers, *Symbol-based multigrid methods for Galerkin B-spline isogeometric analysis*, SIAM J. Numer. Anal. **55** (2016), no. 1, 31–62.
6. C. Douglas, G. Haase, and U. Langer, *A tutorial on elliptic pde solvers and their parallelization*, Society for Industrial and Applied Mathematics, 2003.
7. C. Hofer, S. Takacs, A. Mantzaflaris, et al., *G+Smo*, http://gs.jku.at/gismo, 2018.
8. C. Hofreither and S. Takacs, *Robust multigrid for isogeometric analysis based on stable splittings of spline spaces*, SIAM J. on Numerical Analysis **4** (2017), no. 55, 2004–2024.
9. C. Hofreither, S. Takacs, and W. Zulehner, *A robust multigrid method for isogeometric analysis in two dimensions using boundary correction*, Comp. Meth. in Appl. Mech. Eng. **316** (2017), 22–42.
10. T. J. R. Hughes, J. A. Cottrell, and Y. Bazilevs, *Isogeometric analysis: CAD, finite elements, NURBS, exact geometry and mesh refinement*, Comp. Meth. in Appl. Mech. Eng. **194** (2005), no. 39-41, 4135–4195.
11. S. K. Kleiss, C. Pechstein, B. Jüttler, and S. Tomar, *IETI – Isogeometric tearing and interconnecting*, Comp. Meth. in Appl. Mech. Eng. **247–248** (2012), 201–215.
12. G. Sangalli and M. Tani, *Isogeometric preconditioners based on fast solvers for the Sylvester equation*, SIAM J. Sci. Comput **38** (2016), no. 6, A3644–A3671.
13. S. Takacs, *Robust approximation error estimates and multigrid solvers for isogeometric multipatch discretizations*, (2017), Submitted. https://arxiv.org/abs/1709.05375.